CHAPTER 1

Structures of the Prokaryotic Mechanosensitive Channels MscL and MscS

Stefan Steinbacher,[1] Randal Bass,[2] Pavel Strop,[3] and Douglas C. Rees
Division of Chemistry and Chemical Engineering 114-96, Howard Hughes Medical Institute, California Institute of Technology, Pasadena, California 91125

I. OVERVIEW

The prokaryotic mechanosensitive channels of large (MscL) and small (MscS) conductance respond directly to tension applied to the bacterial membrane. Crystal structures of the *Mycobacterium tuberculosis* MscL and

[1]Present address: Proteros Biostructures GmbH, D-82152, Am Klopferspitz 19, Martinsried, Germany.
[2]Present address: Department of Analytical Sciences, Amgen Inc., 1201 Amgen Court West, Seattle, Washington 98119.
[3]Present address: Howard Hughes Medical Institute, Department of Molecular and Cellular Physiology, E300 Clark Center, Stanford University, Stanford, California 94305.

Current Topics in Membranes, Volume 58 1063-5823/07 $35.00

DOI: 10.1016/S1063-5823(06)58001-9

Escherichia coli MscS were initially reported at 3.5- and 3.9-Å resolutions, respectively. In subsequent refinements described in this chapter, sequence register errors have been corrected to produce improved models for both channels. The pentameric MscL and heptameric MscS are each organized into transmembrane and cytoplasmic domains, although their detailed architectures are distinct in terms of polypeptide folds and oligomeric states. The basic structural framework of the MscL and MscS transmembrane domains is provided by α-helices; each subunit of MscL has 2 helices for a total of 10, whereas MscS has 3 helices per subunit for a total of 21. In contrast to the common architectural theme of helix packing evident in the transmembrane domains, the cytoplasmic domains of MscS and MscL are markedly different in terms of both overall size and polypeptide fold. The permeation pathways in both structures are formed by the right-handed packing of helices that create funnel-shaped pores constricted near the cytoplasmic side by the side chains of hydrophobic residues. From considerations of the relationship between pore geometry and conductance, it is likely that both channel structures represent closed states.

II. INTRODUCTION

Membrane integrity is vital to cellular growth and survival. Among the insults that may be experienced by organisms are changes in external osmolarity; concentration differences of only 10 mM can generate osmotic pressure differences of $\sim$0.2 atm that may rupture membranes of radii $\sim$3 μm (Hamill and Martinac, 2001). Cells immersed in environments that can encounter even modest osmolarity changes must consequently be able to respond on a sufficiently rapid timescale to prevent lysis. Osmotic downshock conditions, such as the sudden exposure of a bacteria to rain or other source of freshwater, represent a particularly challenging situation (Booth and Louis, 1999; Poolman *et al.*, 2002). Without safety-value mechanisms to release cellular contents (Britten and McClure, 1962), cells would not be able to withstand the resultant turgor pressures of tens to hundreds of atmospheres associated with the influx of water. Through the pioneering efforts of C. Kung and coworkers (Martinac *et al.*, 1987; Sukharev *et al.*, 1994, 1997), the proteins in bacteria responsible for sensing the increase in membrane tension accompanying osmotic downshock have been identified. These proteins form high-conductance channels in the inner membrane that can open and close in direct response to tension applied to the bilayer. Such properties are consistent with a biological role for these channels in responding to sudden increases in turgor pressure to jettison water and other cellular contents to prevent cell lysis during hypoosmotic shock. To date, two

general families of these channels have been identified, the mechanosensitive channel of large conductance (MscL) (Sukharev *et al.*, 1994) and of small conductance (MscS) (Levina *et al.*, 1999). Reviews of these channels have appeared (Perozo and Rees, 2003; Strop *et al.*, 2003; Sukharev and Corey, 2004; Blount *et al.*, 2005; Booth *et al.*, 2005; Sukharev *et al.*, 2005) that emphasize different aspects of these channels. Although they are relatively simple, intrinsically stretch-activated systems, the basic principles of how MscL and MscS sense forces applied to the lipid bilayer likely reflect the mechanisms underlying such diverse cellular phenomena as touch, hearing, gravity, and pressure (Kung, 2005).

From a structural perspective, MscL and MscS represent fascinating targets as they provide an opportunity to explore the coupling between protein conformation and the membrane environment responsible for channel gating. Tension and pressure sensitive systems, such as MscL and MscS, have the added attraction that these environmental properties are energetically coupled to changes in protein area and volume, respectively, which may be directly quantitated from structural models. The crystallographic analyses of the *M. tuberculosis* MscL (Chang *et al.*, 1998) and the *E. coli* MscS (Bass *et al.*, 2002) described in this chapter were motivated by these considerations to provide the structural frameworks essential for a mechanistic understanding of mechanosensitive systems at the molecular level.

III. CONDUCTANCES OF MscL AND MscS: GENERAL CONSIDERATIONS

The conductance of a channel, g, describes the coupling between the current flow through the channel, I, and the driving force across the membrane, V, in the Ohm's Law expression:

$$gV = I \tag{1}$$

where g is the inverse of the channel resistance. When I and V are expressed in amperes and volts, respectively, the units of g are siemens (S) which are equivalent to reciprocal ohms. The conductances of MscL and MscS have been reported as ~3 and 1 nS, respectively (Sukharev *et al.*, 1997, 1999; Levina *et al.*, 1999), when measured in solutions containing 200-mM KCl and 40- to 90-mM $MgCl_2$. With a potential difference of 100 mV, a conductance of 1.6 nS equals 160 pA, which is equivalent to the flow of $\sim 10^9$ ions/s across the membrane. These are quite high-conductance channels; for comparison, K^+ channels and the acetylcholine receptor have conductances that are ~100 times smaller than MscL (Hille, 2001). While these conductances reflect the properties of the fully open state, subconductance states have been reported for both channels (Sukharev *et al.*, 1999; Shapovalov and

Lester, 2004; Akitake *et al.*, 2005). An inactivated state of MscS has also been described (Akitake *et al.*, 2005). From conductance measurements in the presence and absence of different size molecules, the pore radius in the open state of MscL has been estimated in the range of 15–20 Å (Cruickshank *et al.*, 1997; Sukharev *et al.*, 1999, 2001b). As anticipated from the high conductances, both channels are essentially nonselective, although MscS does exhibit a slight preference for anions (Martinac *et al.*, 1987; Sukharev, 2002).

The conductance of a channel reflects, among other factors, the geometry of the permeation pathway (Hille, 2001). Viewed as a continuum model, the conductance of a channel will vary linearly with the cross-sectional area and inversely with the length of the permeation pathway. The conductance of real channels will, of course, depend on molecular details that cannot be captured in a continuum model. One interesting example is the observation in molecular dynamics simulations that hydrophobic pores of diameter smaller than 4.5 or 6.5 Å are closed to water and ions, respectively—that is, nonconducting channels need not be geometrically closed (Beckstein and Sansom, 2004). Consequently, even qualitative analyses of low conductance, selective ion channels will likely require detailed calculations. For high conductance, nonspecific channels, however, such as MscL with estimated pore radii greater than 10 Å in the open state, macroscopic, continuum models may not be a bad approximation, at least for a qualitative understanding of the dependence of channel conductance on the geometry of the permeation pathway. It is in this spirit that the following analysis is presented by way of background to help functionally interpret the MscL and MscS structures.

In the simplest continuum model for the conductance of a cylindrical channel of radius r and length l, the conductivity is given by (Edmonds, 2001; Nelson, 2004):

$$g = \frac{cDq^2}{k_B T}\frac{\pi r^2}{l} \tag{2}$$

where c, q, and D denote the concentration, electronic charge, and diffusion coefficient for the univalent permeant ion, respectively; k_B is the Boltzmann constant and T is the temperature. When c is expressed in molar concentration units, r and l in Ångstroms, and taking $D = 2 \times 10^{-5}$ cm^2/s for KCl at 298 K (Robinson and Stokes, 1959), this expression reduces to

$$g = 2.4\frac{cr^2}{l}\,(\text{nS}) \tag{3}$$

Macroscopic models of this type have been found to overpredict the experimentally measured conductance of channels by factors of ~5–6 (Smart *et al.*, 1997), resulting in an empirical expression for g_{eff}:

$$g_{\text{eff}} \sim 0.4 \frac{cr^2}{l} (\text{nS}) \tag{4}$$

with $r = 15$ Å, $l = 30$ Å, and $c = 0.3$ M, $g_{\text{eff}} \sim 0.9$ nS.

Macroscopic models may also be used to estimate the volume of water and other cellular contents flowing through an open mechanosensitive channel driven by an osmotic pressure gradient. The volume per unit time, J, of a fluid of viscosity η flowing through a macroscopic pipe of radius r and length l, under a pressure differential ΔP is given by the Hagen–Poiseuille equation (Denny, 1993):

$$J = \frac{\pi r^4}{8\eta} \frac{\Delta P}{l} \tag{5}$$

For a mechanosensitive channel, approximated as $r = 15$ Å and $l = 30$ Å, experiencing an osmotic pressure gradient of $\Delta P = 0.1$ atm $= 1.013 \times 10^5$ dyne/cm^2, and given the viscosity of water as $\eta = 0.01$ g/cm s, the volume flow through the pipe may be calculated from Eq. (5) as $J = 6.7 \times 10^{-15}$ cm^3/s, which corresponds to 2.2×10^8 waters/s (from the average molecular volume for water ~ 30 Å$^3 = 3 \times 10^{-23}$ cm^3). For comparison, the permeation rate through the aquaporin water channel is $\sim 10^9$ waters/s (Zeidel *et al.*, 1992).

For a cell experiencing osmotic downshock, the volume flow of water per unit time (J_{V}) across a membrane of surface area A in response to an osmotic pressure gradient, ΔP, is given by (Weiss, 1996):

$$J_{\text{V}} = L_{\text{V}} \text{A} \Delta P \tag{6}$$

where L_{V} is the hydraulic conductivity. An approximate value of L_{V} for biological membranes is $\sim 10^{-5}$ cm/s atm. If an osmotic pressure gradient is imposed across a membrane containing N_{C} channels that support a volume flow given by the Hagen–Poiseuille equation, then the equilibrium condition where the flow across the membrane [Eq. (6)] is balanced by the flow through the channels [Eq. (5)] becomes:

$$\begin{aligned} L_{\text{V}} A \Delta P &= N_{\text{C}} \frac{\pi r^4}{8\eta l} \Delta P \\ \frac{N_{\text{C}}}{A} &= \frac{8 L_{\text{V}} \eta l}{\pi r^4} \end{aligned} \tag{7}$$

With the parameters defined as above, $N_{\text{C}}/A \sim 5 \times 10^7$ channels/cm^2. For a spherical cell of radius $\sim 10^{-4}$ cm (approximating *E. coli*), $A \sim 10^{-7}$ cm^2 or $N_{\text{C}} \sim 5$ channels per cell. Experimental estimates from electrophysiological analyses suggest there are 4–5 MscL and 20–30 MscS channels per *E. coli* (Stokes *et al.*, 2003). An important conclusion from this analysis is that mechanosensitive channels with $r \sim 15$ Å in the open state are anticipated

to have approximately nanoSiemens conductances and support volume flows that are consistent with the observed biological properties of these channels.

IV. STRUCTURE DETERMINATION OF MscL AND MscS

A. General Considerations in Membrane Protein Crystallography

While the details vary, the basic steps in the structure determination of MscL and MscS generally mirror those employed in the crystallographic analysis of most membrane proteins, starting with the bacterial photosynthetic reaction center (Deisenhofer *et al.*, 1985). These steps may be somewhat arbitrarily classified as: (i) obtaining a suitable source for the membrane protein of interest, (ii) solubilization from the membrane, (iii) purification, (iv) crystallization, and (v) structure solution. A brief overview of these steps, noting aspects relevant to MscL and MscS, follows. A more detailed description of the MscL structural analysis can be found in Spencer *et al.* (2003).

1. Source of Membrane Protein

It is no coincidence that the membrane proteins whose structures were first determined occurred naturally at high abundance in appropriate sources. Indeed, the first structures of recombinantly expressed membrane proteins, the prokaryotic channels KcsA (Doyle *et al.*, 1998) and MscL (Chang *et al.*, 1998) were determined in 1998, some 13 years after the reaction center. Since most membrane proteins are found in very low abundance, recombinant methods are essential for their structure determination. Not only do recombinant methods allow overproduction in increased quantities, but they also enable membrane proteins from many different species to be produced and over-expressed. In addition, they can be prepared with different affinity tags to facilitate rapid and efficient purification. A wide variety of overexpression systems have been utilized or proposed for membrane proteins (Grisshammer and Tate, 1995, 2003). However, the most successful expression system has been based on *E. coli* (Drew *et al.*, 2003), which has been almost exclusively utilized for crystal structure analyses of recombinant prokaryotic membrane proteins, including MscL and MscS. Prokaryotic systems enjoy a number of significant advantages for membrane protein work; in particular, the cells can be easily grown on a large scale, and the growth conditions and induction strategies can be manipulated to obtain sufficient quantities of purified protein to facilitate screening and refinement of crystallization conditions.

2. Solubilization

Solubilization of integral membrane proteins from the phospholipid bilayer for crystallization studies is typically achieved through detergent extraction (Michel, 1991; Iwata, 2003). This results in the formation of protein–detergent mixed micelles where the hydrophobic region of the protein is solvated by the nonpolar component of the detergent, while the polar component interacts favorably with the aqueous solution. The choice of detergent is crucial; some detergents are too vigorous and will either dissociate oligomeric proteins into subunits or, as in the case of sodium dodecyl sulfate, denature the protein, while others are too mild to efficiently extract the protein from the membrane. Although certain detergents have been used repeatedly in structural analyses (such as dodecylmaltoside used with MscL), identification of the "correct" detergent is still an empirical process involving the screening of several dozen detergents and must be established for each protein.

While detergents are extremely useful for the membrane extraction and homogenous preparation of membrane proteins for structural studies, they are not completely faithful mimics of the bilayer environment. In particular, detergent micelles are typically spherical, in contrast to the planar structure of the bilayer. Among other factors, these distinctions will perturb the lateral pressure profile (Cantor, 1999) experienced by the protein in detergent or the bilayer, which is reflected in a general destabilization of membrane proteins in detergent solutions (Stowell and Rees, 1995; Bowie, 2001; Odahara, 2004; Lee *et al.*, 2005). In addition to these general effects, there can be specific phospholipid–protein interactions that are important for protein stability and function, that can also have a significant impact on crystallization (Zhang *et al.*, 2003; Long *et al.*, 2005; Guan *et al.*, 2006). This is an area that will clearly benefit from more careful quantitative analysis of the lipid content of membrane protein preparations.

3. Purification

The use of affinity tags has revolutionized the process of protein purification, including membrane proteins (Kashino, 2003). Ideally, the detergent-solubilized material can be adsorbed to column material with a high affinity for the tag, which after washing can be eluted by an increased concentration of the appropriate ligand. Most frequently, affinity tags composed of multiple histidines, typically 6–12, have been employed for purification with immobilized metal affinity columns and subsequent elution with imidazole; in the cases of MscL and MscS, the tags contained 10 histidines. Other affinity tag purification systems are also available (Terpe, 2003). Additional purification steps such as ion exchange or gel filtration chromatography can improve purity, although sometimes these steps have a negative effect on

crystallization, presumably due to loss of phospholipids. Gel filtration chromatography and light scattering can be very helpful in characterizing the monodispersity of a sample. Detergent solubilized material can form a variable extent of high-molecular-weight species (soluble aggregates) that are not suited for crystallization; this was a particular problem with MscL due to the apparent formation of MscL–MscL dimers (i.e., a species with a total of 10 subunits).

4. Crystallization

The strategy for production of three-dimensional crystals of membrane proteins closely mirrors that for water-soluble proteins; sets of conditions with varying concentrations and types of precipitants, salts, and buffers (pH) are screened, typically by vapor diffusion methods, for initial leads that are then optimized. An informative analysis of membrane protein crystallization is presented in Iwata (2003).

With a few notable exceptions, crystals of integral membrane proteins are typically of modest diffraction quality. This is likely a consequence of two factors: the generally high solvent content of membrane protein crystals and the destabilization of membrane proteins in detergent solutions. The high solvent content reflects the presence of the detergent micelle surrounding the apolar regions of the protein surface, which inhibits participation of this region in lattice contacts. For the membrane protein data presented in Fig. 1, the average Matthews coefficient (V_m) (Matthews, 1968) for a membrane protein is ~4 Å^3/Da, which corresponds to ~70% solvent; this may be compared to the average of 2.6 Å^3/Da for water-soluble proteins (Kantardjieff and Rupp, 2004), which corresponds to ~50% solvent. In both cases, there is a trend that the diffraction resolution is correlated with V_m. Of particular note, both MscL and MscS have $V_m \sim 6$ Å^3/Da, which indicates these crystals have high solvent contents, even for membrane proteins, and this may be correlated with the observed "modest" diffraction quality of the crystals.

5. Structure Determination

The crystal structure determination of membrane proteins involves the same general considerations as for any other sample. Other than data collection, the main barrier is phase determination; for MscL, this involved preparation of suitable heavy atom derivatives for the method of multiple isomorphous replacement, while it was possible to incorporate selenomethionine into MscS which permitted phase determination using the multiple wavelength anomalous diffraction phasing method. The main technical issues in the crystallographic analyses of membrane proteins reflect their typically (but not exclusively) modest resolution and associated high B factors (see Section IV.B). Advances

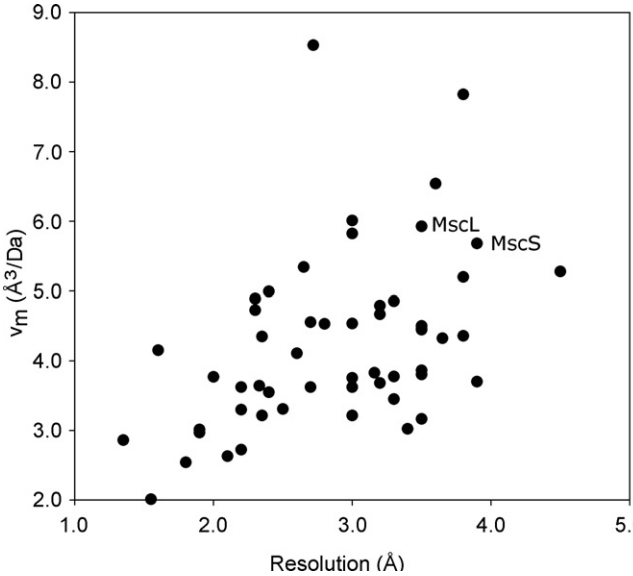

FIGURE 1 Distribution of the Matthews coefficient (V_m) and the crystallographic resolution for integral membrane proteins of known structure. Entries were taken from the database of S. White (http://blanco.biomol.uci.edu/membrane_proteins_xtal.html; White, 2004). A general trend is evident that structures with higher V_m (greater solvent content) tend to diffract more poorly than structures with lower V_m and consequently a lower solvent content. The points corresponding to the MscL and MscS structures are indicated.

in synchrotron beam lines, including automated sample handling and data collection, and refinement algorithms have significantly enhanced the ability to extract useful data from weakly diffracting crystals.

B. Crystallographic Analysis of MscL and MscS

The *M. tuberculosis* MscL and *E. coli* MscS structures were originally reported in 1998 and 2002 (Chang *et al.*, 1998; Bass *et al.*, 2002), and deposited in the Protein Data Bank (http://www.rcsb.org/pdb; Berman *et al.*, 2000) as entries 1MSL and 1MXM, respectively. The diffraction data for both structures were characterized by a rapid decrease in intensity with resolution, associated with large values for the overall temperature factors of $\sim$100 Å^2. As a result, while the diffraction data were very strong at low resolution, the average intensity quickly decreased with increasing resolution

as reflected in the limiting resolutions of 3.5 and 3.9 Å for MscL and MscS, respectively. While the experimentally phased electron density maps fortunately appeared to be of much better quality than would be expected for this overall temperature factor, it was difficult to obtain well-refined models. In the case of MscL, we initially were unable to refine any single model to values of R and R_{free} below ~0.40 and 0.42, respectively, and consequently a "multiple structures" strategy was implemented where nine copies of the structure were refined again the native data to final R and R_{free} values of 0.26 and 0.35. The refinement of MscS was better behaved in that a single structure could be refined against the native data to R and R_{free} values of 0.33 and 0.36, respectively, although these values are still higher than desirable.

Despite extensive efforts, we have been unable to improve the diffraction quality of MscL and MscS crystals beyond those originally described. Consequently, we decided to reanalyze the original data to see if improved structural models could be produced. Following reprocessing of the diffraction data to 3.5- and 3.7-Å resolution for MscL and MscS, respectively, electron density maps for model building and refinement were generated by calculating phases from the PDB coordinates to ~16-Å resolution. Using noncrystallographic symmetry averaging (five- and sevenfold for MscL and MscS, respectively) and solvent flattening, the phases were refined and incrementally extended over 200 steps to their limiting resolutions. As a consequence of the high degree of noncrystallographic symmetry and high solvent content, this procedure led to a significant improvement in the quality of the final electron density maps that facilitated rebuilding of the models. While the overall folds of the polypeptide chains were unchanged, register errors were detected and corrected in both MscL and MscS. A critical aspect in the refinement was the parameterization of the bulk solvent correction that is crucial for the proper scaling between observed and calculated structure factors at very low resolution. As these reflections are quite strong, small differences in scaling can significantly influence the resulting electron density maps, particularly in regions of the protein surface. The revised models have been refined to final values of R and R_{free} of 0.319 and 0.338 for MscL, and 0.293 and 0.321 for MscS; while still high, they do represent a significant improvement over the original models and are a reasonable reflection of the quality of structural models at these resolutions. The Protein Data Bank entries for the revised coordinates of MscL and MscS are 2OAR and 2OAU, respectively.

Relative to the 1MSL coordinate set, the most significant changes in the revised MscL structure are the modeling of the first 12 residues (missing in the original model) as an α-helix, the complete rebuilding of the periplasmic

loop, and correction of a six-residue register error in the cytoplasmic helix. When structurally equivalent residues are compared between the original and revised models, the overall root mean square (rms) deviation in Cα positions is 1.5 Å. If the sequence register corrections are not taken into account, the rms deviation increases to 8.7 Å for all residues (10–118) in the initial model (primarily due to the 6-residue register shift in the cytoplasmic helix), with an rms deviation of 1.8 Å for residues in the membrane-spanning helices (15–43 and 69–89). Relative to the 1MXM model, the most significant changes in the revised MscS structure are adjustment for the deviations from exact noncrystallographic symmetry in the membrane-spanning region, including rebuilding of the loop between TM2 and TM3, and correction of the sequence register for residues 160–195 and 226–244. One consequence of the deviations from sevenfold symmetry in the membrane-spanning domain of MscS is that the permeation pathway more closely resembles a pinched tube. When all structurally equivalent residues in the two MscS models are superimposed, the overall rms deviation in Cα positions is 1.4 Å; without correcting for the register errors, the rms deviation increases to 3.4 Å for all residues (27–280) in the model, and is 2.2 Å for residues in the second and third transmembrane helices. There is relatively little change between the original and revised models in the permeation pathways of both MscL and MscS.

V. MscL AND MscS STRUCTURES

MscL and MscS exist as pentamers and heptamers, respectively, with the permeation pathway surrounding the axis of rotational symmetry in the center of each channel. Although they share a common organization of an N-terminal transmembrane domain and a C-terminal cytoplasmic domain, the overall arrangements of the polypeptide folds are distinct, indicating that they do not share a common evolutionary ancestor. In the subsequent discussion, unless otherwise specified, residue numbers refer to the *M. tuberculosis* MscL or *E. coli* MscS sequences as appropriate.

The polypeptide fold of an MscL subunit (Fig. 2A) exhibits a simple topology containing two membrane-spanning helices (TM1 and TM2) and a cytoplasmic α-helix near the C-terminus. Starting from the conserved cytoplasmic N-terminus, residues 1–12 of each subunit adopt an α-helical conformation that would likely be positioned at the cytoplasmic surface of the membrane. TM1 (residues 13–47) crosses the membrane toward the periplasm and creates the permeation pathway through formation of a right-handed helix bundle with the symmetry related TM1s from the other

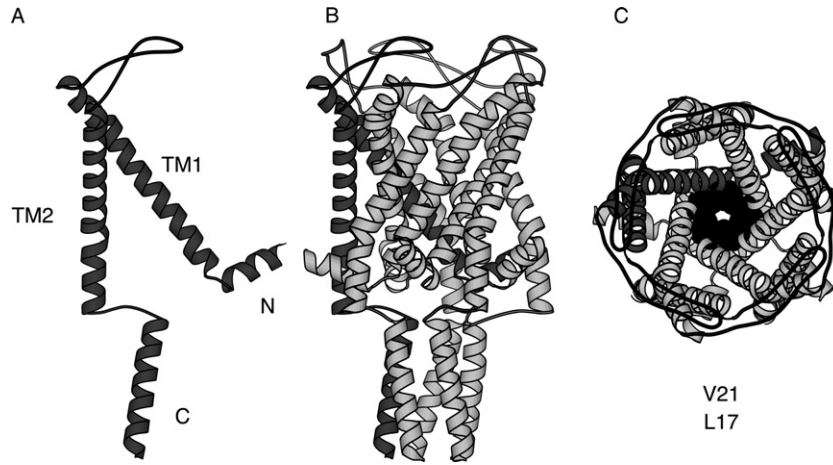

FIGURE 2 Ribbons diagram representations of the MscL channel. (A) The polypeptide fold of an individual MscL subunit viewed from the plane of the membrane, with the positions of the two membrane-spanning helices, TM1 and TM2, indicated. The termini of the channel are designated by "N" and "C," respectively. (B) The MscL pentamer viewed in the same orientation as (A). (C) The membrane-spanning region of MscL viewed down the membrane normal from the periplasm. The side chains of Leu17 and Val21 that constrict the permeation pathway are shown as black CPK models. The subunit illustrated in (A) is shaded dark, while the remaining subunits are light in these panels. Ribbons representations in this chapter were prepared with MOLSCRIPT (Kraulis, 1991).

subunits (Fig. 2B and C). Residues 48–68 form an extended loop with poor density in the periplasm that approximates two antiparallel β-strands. TM2 (residues 69–101) then returns to the cytoplasm along the exterior of the channel to complete the membrane-spanning domain of MscL. Within the transmembrane domain, each TM1 helix interacts with four surrounding helices: two TM1 helices from adjacent subunits (helix crossing angle $\sim -42°$) and two TM2 helices, one from the same subunit (crossing angle $\sim 134°$) that contacts the periplasmic half of TM1 and the other from an adjacent subunit (crossing angle $\sim -175°$) that contacts the more cytoplasmic half of TM1. Although there are no contacts between pairs of TM2 helices, the subunits are further interconnected in the transmembrane domain by the threading of the N-terminal helix of one subunit between the TM1 and TM2 helices of a neighboring subunit. The membrane and cytoplasmic domains are connected by a short linker leading to a cytoplasmic helix (106–125) in each subunit that associates with the symmetry related mates to form a left-handed (crossing angle $\sim +20°$), five-helix bundle. Of particular note, the periplasmic loop and the cytoplasmic helix in the revised

crystal structure now more closely resemble the model proposed by Guy and Sukharev in their analysis of MscL gating (Sukharev *et al.*, 2001a,b).

While the helix packing arrangement in the membrane-spanning domain of MscS is also relatively simple, the overall topology of the polypeptide fold in the cytoplasmic domain is considerably more complex than observed for MscL (Fig. 3A and B). Each subunit of MscS contains three membrane-spanning helices. In contrast to MscL, the N-terminus of MscS is periplasmic, with TM1 (residues 27–60) crossing the bilayer on the exterior of the channel, TM2 (residues 63–90) forming a central layer, and TM3 (93–128) returning to the cytoplasm through the channel interior. The TM1 and TM2 helices within one subunit are packed together in an antiparallel fashion (crossing angle $\sim 165^\circ$) that buries an extensive interface, but makes few contacts with other helices in the membrane-spanning domain and has relatively weak density. The permeation pathway (Fig. 3C) is formed by the packing of adjacent TM3 helices to form a right-handed helix bundle (packing angle $\sim -22^\circ$). A pronounced kink is present in the TM3 helix near Gly113 which results in the axis of the C-terminal end of this helix being

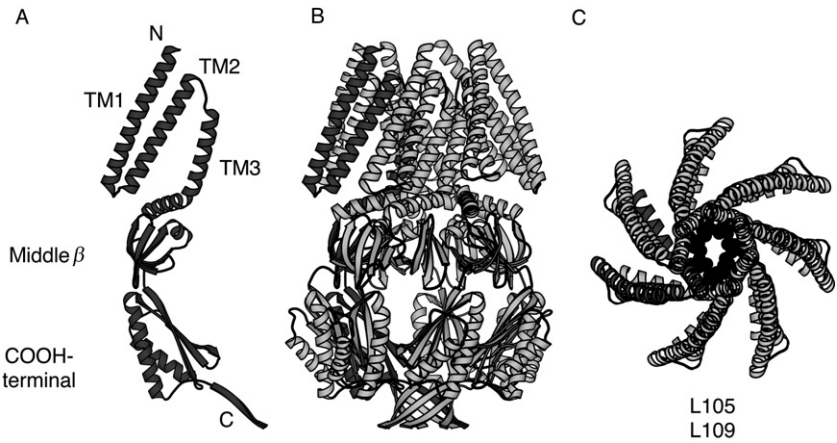

FIGURE 3 Ribbons diagram representations of the MscS channel. (A) The polypeptide fold of an individual MscS subunit viewed from the plane of the membrane, with the positions of the three membrane-spanning helices, TM1, TM2, and TM3, indicated. The termini of the channel are designated by "N" and "C," respectively, as are the "middle β" and "COOH-terminal" domains of the cytoplasmic region of MscS. (B) The MscS heptamer viewed in the same orientation as (A). (C) The membrane-spanning region of MscS viewed down the membrane normal from the periplasm. The side chains of Leu105 and Leu109 that constrict the permeation pathway are shown as black CPK models. The oval shape of the pore reflects deviations from exact sevenfold symmetry in this region. The subunit illustrated in (A) is shaded dark, while the remaining subunits are light in these panels.

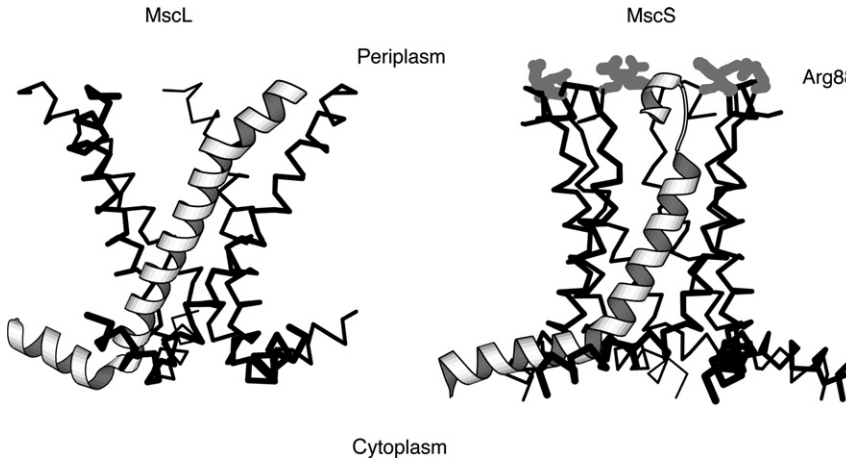

FIGURE 4 The permeation pathways of MscL (left) and MscS (right), defined by the N-terminal helix and TM1 of MscL and TM3 of MscS, as viewed from the membrane. One subunit is depicted in ribbons representation for each structure, while the symmetry-related structures are shown as Cα traces. This figure illustrates how the pore-forming helix in both structures connects directly to a helix likely positioned in the cytoplasmic surface of the membrane. The locations of Arg88 that may contribute to the anionic preference of MscS are shown as gray ball-and-stick models on the periplasmic surface.

oriented nearly perpendicular to the membrane normal. It is likely that this region of TM3 extends out of the membrane and is positioned at the headgroup-aqueous interface. Intriguingly, although the polarity of the polypeptide chain is reversed, this feature resembles the N-terminal and TM1 helices of MscL in that a helix positioned at the cytoplasmic membrane surface is directly connected to the helix lining the permeation pathway (Fig. 4).

The minimal interaction between the TM1–TM2 helical hairpin and the rest of MscS, particularly the permeation pathway formed by TM3, is somewhat surprising, and suggests the possibility that this more loosely packed state may be stabilized by detergent (foscholine-14). As a consequence of the lateral pressure profile in the bilayer, a reasonable expectation for when MscS is embedded in a membrane is that the TM1–TM2 helices would be tightly packed against the permeation pathway, which is not observed. This situation is reminiscent of the behavior of the voltage sensor in the KvAP K^+ channel structure (Jiang *et al.*, 2003; Lee *et al.*, 2005); indeed, there are intriguing similarities between these two elements of MscS and K^+ channels (Bass *et al.*, 2003), including the presence of multiple arginine residues in a membrane embedded helical hairpin. In view of the initial report that MscS was voltage sensitive (Martinac *et al.*, 1987), it was

suggested that the arginine residues present in TM1 and TM2 might be responsible for this dependence (Bass *et al.*, 2002). Subsequent studies have indicated that the voltage dependence of MscS is considerably more complex than originally envisioned and likely has little effect on the closed to open transition (Akitake *et al.*, 2005). Nevertheless, these common features between the K^+ channel voltage sensor and the TM1–TM2 hairpin of MscS are suggestive that arginine-rich helices are conformationally sensitive elements that are energetically poised to move relative to the membrane in response to environmental changes (Hessa *et al.*, 2005).

The cytoplasmic domain of MscS is quite extensive relative to MscL, with the most notable structural feature being the large interior chamber of ~40-Å diameter that connects to the cytoplasm through multiple openings. The protein framework that encloses this chamber is generated by two domains of each subunit, termed middle-β and COOH-terminal. The middle-β domain is organized around a β-sheet that connects with those from other subunits to form a continuous β-sheet structure that extends around the entire protein. As noted by Mura *et al.* (2003), this arrangement exhibits a striking resemblance to the heptameric Sm proteins involved in mRNA processing in terms of both the subunit fold and oligomeric organization. The β-sheet in this domain is twisted 180°; as a consequence of the odd number of subunits in MscS, the continuous sheet forms the equivalent of a molecular Mobius strip since it twists 3.5 times in one complete cycle around the cytoplasmic domain of MscS. The cytoplasmic domain is completed by the COOH-terminal domain that exhibits a mixed α/β-structure assigned to the ferredoxin fold family in the SCOP database (Murzin *et al.*, 1995). The entire heptameric assembly is linked at the C-terminus by a seven-stranded parallel β-barrel that contains one strand from each subunit.

VI. THE PERMEATION PATHWAY IN MscL AND MscS

The permeation pathway across the membrane is dominated by the packing of symmetry related helices, either TM1 in MscL (Fig. 2C) or TM3 in MscS (Fig. 3C), into a right-handed bundle. The striking pattern of conserved Gly and Ala noted in MscL and MscS (Levina *et al.*, 1999) corresponds to residues localized at these helix–helix packing interfaces. The lining of the pore with a right-handed helical arrangement is not a unique feature of mechanosensitive channels and a similar organization has been observed in other systems, including members of the K^+ channel (Doyle *et al.*, 1998) and aquaporin families (Fu *et al.*, 2000; Murata *et al.*, 2000). The general shape and size of the helical framework surrounding the permeation pathway reflects the molecular symmetry, the helix–helix crossing angle (α)

and the tilt of the helix axis (η) with respect to the membrane normal (taken to coincide with the symmetry axis). With ideal helices and exact N-fold rotational symmetry, these parameters are not all independent but are related by the expression (Spencer and Rees, 2002)

$$\cos \alpha = \cos^2 \eta + \sin^2 \eta \cos \theta \tag{8}$$

where $\theta = 2\pi/N$. Values of these parameters for the helices surrounding the pores in MscL, MscS, and KcsA are provided in Table I, and it may be seen that the helix–helix crossing angles calculated from this equation are in good agreement with the values observed in these structures. An interesting question concerns how the oligomeric state is specified; for example, the crossing angles of MscL and KcsA agree to within 3°, and the tilt angles within 4°, yet the former is a pentamer while the latter is a tetramer. Presumably this behavior reflects the pattern of residues, particularly Gly and Ala, along the helix packing interface, although this code cannot yet be deciphered.

The permeation pathways of both MscL and MscS are roughly funnel shaped with the larger opening facing the periplasmic surface of the membrane and the narrowest point near the cytoplasm. A more quantitative analysis of the pore geometry by the program HOLE (Smart *et al.*, 1996) reveals that the pore in MscL varies from a radii of ~15 Å at the periplasm, to the narrowest point of <1 Å at the hydrophobic plug; the corresponding values in MscS are ~14 and ~2.5 Å. The latter distance is smaller than the

TABLE I

Packing Geometries of Helices Lining the Permeation Pathways of MscL, MscS, and KscA[a]

Channel	N	Tilt angle η	Crossing angle α	Crossing angle α calculated [Eq. (8)]	Packing distance
MscL	5	36.8°	−41.5°	±41.2°	7.5 Å
		(36.1–37.5°)	(−40.7 to −42.3°)		(7.2–7.7 Å)
MscS	7	26.0°	−23.7°	±21.9°	8.2 Å
		(24.4–27.2°)	(−21.6 to −27.3°)		(8.0–8.4 Å)
KscA	4	33.0°	−44.5°	±45.3°	7.6 Å

[a]The relevant helices are defined by residues 13–36, 95–110, and 86–121 of MscL, MscS, and KcsA, respectively. The revised coordinates described in this chapter were used for the structures of MscL and MscS, while PDB entry 1K4C was used for KcsA (Zhou *et al.*, 2001). The crossing angle and packing distances were calculated by the program PROMOTIF (Hutchinson and Thornton, 1996), while the tilt angle was defined as the angle between the helix axis and the symmetry axis of the channel, assumed to coincide with the membrane normal.

minimum radius of 5.5 Å originally reported for MscS and reflects the deviations from noncrystallographic symmetry observed in the pore region which resembles a pinched hose. Consequently, it is likely that the structure of MscS corresponds to the closed state as proposed by Sukharev and coworkers (Anishkin and Sukharev, 2004). At their narrowest point, the pores are constricted by the side chains of symmetry-related residues: Leu17 and Val21 in MscL, and Leu105 and Leu109 in MscS. Hydrophobic plugs have been similarly noted in the acetylcholine receptor (Miyazawa *et al.*, 2003) and K^+ channels (Doyle *et al.*, 1998; Kuo *et al.*, 2003), and may allow the channel to maintain a closed state without being completely shut geometrically (Beckstein and Sansom, 2004).

The interior of the permeation pathway in MscL is predominantly lined by the side chains of polar residues in TM1: Thr25, Thr28, Ala29, Thr32, Lys33, Thr35, Asp36, and Thr40. In contrast to the TM1 residues involved in helix–helix contacts, these residues are not so highly conserved. While TM1 residues provide the major surface area contribution to the lining of the pore, residues from TM2, in particular Asp68, Val71, Ser75, and Asn78, also contribute to the pore lining. While these residues are not highly conserved, they do tend to be polar. In contrast to MscL, residues from TM3 lining the permeation pathway in MscS have a more apolar character. Of these residues, Gln92, Ala94, Leu97, Ala98, Leu105, Leu109, and Gln112, only the two glutamines are polar, a characteristic that tends to be conserved in MscS homologues. Adjacent to this region, at the C-terminal end of TM2, Arg88 residues are positioned with their positively charged side chains surrounding the permeation pathway (Fig. 4). Although there is no direct experimental evidence for this yet, it is plausible that this residue contributes to the preference of MscS for anion conductance.

VII. DISULFIDE BOND FORMATION IN MscL

As exemplified by studies on MscL (Sukharev *et al.*, 2001a; Betanzos *et al.*, 2002; Levin and Blount, 2004), chemotaxis receptors (Pakula and Simon, 1992; Bass and Falke, 1999) and LacY (Wu and Kaback, 1996), disulfide trapping provides an important approach for the analysis of structure and dynamics in membrane protein systems. With the availability of the *M. tuberculosis* MscL structure, we prepared a series of MscL variants having single cysteines substituted at every position in TM1 and TM2 to directly assess disulfide bond formation in a structurally characterized membrane protein system. (The wild-type protein lacks cysteine residues.) Following purification of MscL via solubilization with dodecylmaltoside and purification by nickel-affinity chromatography, each variant was

subjected to mild oxidation with 1-mM Cu(II)-1,10 phenanthroline for 20–30 min at 37°C, followed by quenching of unreacted thiols with *N*-ethylmaleimide. For each position, monomer and disulfide-linked dimers were quantitated following electrophoresis in nonreducing SDS polyacrylamide gels. From the ratio of dimer to monomer in the presence and absence of the Cu(II)-1,10 phenanthroline oxidant, the fraction of cysteines forming disulfide bridges could be determined. Since MscL is a pentamer, at most only $4/5 = 0.80$ of the cysteines can be cross-linked within a given molecule.

As seen from Fig. 5, there is considerable variation in the extent of disulfide bond formation observed for residues in TM1 and TM2. Several observations can be made from these results: disulfide bond formation is observed at every position, including membrane (detergent) exposed residues; disulfide bond formation tends to increase toward the ends of each helix that are closest to the aqueous environment; and within a set of adjacent residues, disulfide bond formation tends to be greater for residues closer to their symmetry mates and lower for residues that are more distant. This latter feature is particularly evident in the absence of added oxidant; under these conditions, there is a distinct preference for disulfide bond formation to occur in the membrane-spanning region only for residues on the side of the helix closest to their symmetry mates. It is also striking that residues separated by over 20 Å in the crystal structure can be cross-linked, which parallels earlier observations on water-soluble proteins (Careaga and Falke, 1992; Butler and Falke, 1996). This behavior emphasizes that disulfide trapping is an effectively irreversible trapping technique, and disulfides will form and accumulate between pairs of distant cysteines if they are brought into proximity by even infrequently occurring conformational fluctuations. Electrophysiological characterization of the variant with Cys substituted at position 15 indicates that these fluctuations occur in an asymmetric form of the open state (Shapovalov *et al.*, 2003).

VIII. CONCLUDING REMARKS

A critical challenge for future structural studies of MscL and MscS is to trap and stabilize these channels in specific functional states, particularly the fully open state. Approaches for achieving this objective are heavily influenced by the pioneering studies of the groups of Sukharev and Guy (Sukharev *et al.*, 2001a,b; Betanzos *et al.*, 2002) and Perozo (Perozo *et al.*, 2002a,b) who have developed an iris-type model for the opening of MscL. Studies on MscS from Booth's group (Edwards *et al.*, 2005) have highlighted rearrangements in the packing interface between TM3 helices that are coupled to channel opening and closing in this system, while a role for the C-terminal

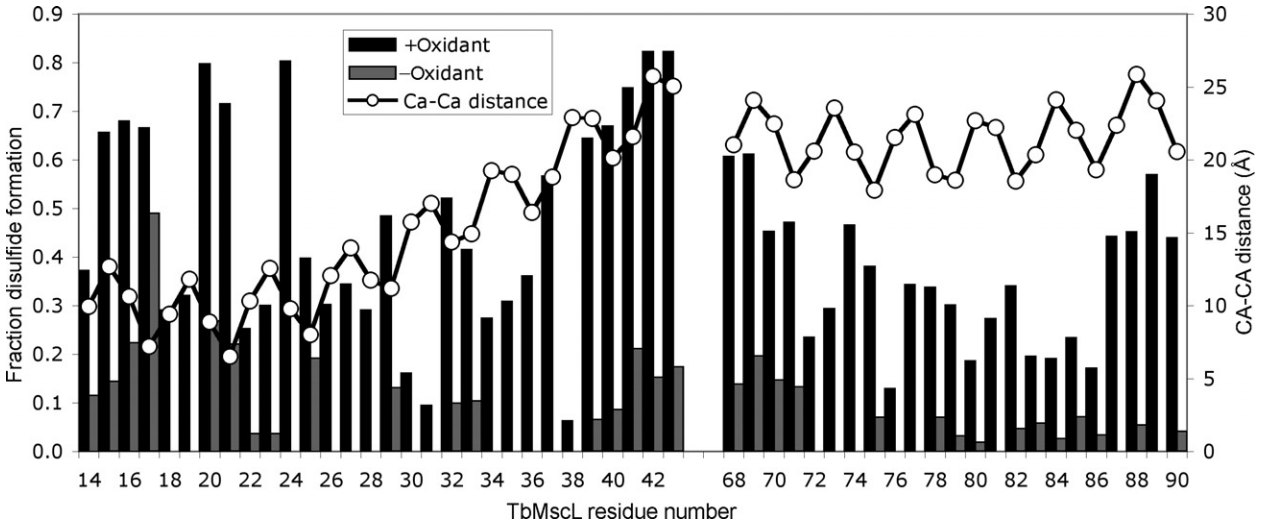

FIGURE 5 Summary of disulfide cross-linking experiments for the *M. tuberculosis* MscL. The fraction of cysteines participating in disulfide bonds in the presence (+oxidant) and absence (−oxidant) of 1-mM Cu(II)-1,10 phenanthroline are shown for each residue in TM1 and TM2 of MscL. Also shown are the distances in Cα positions between adjacent, symmetry-related residues. Within a local set of residues, there is a trend that residues closer to their symmetry-related mates tend to form disulfide bridges to a greater extent than residues that are more distant. This trend is most evident for disulfide formation in TM1 in the absence of oxidant, since little or no disulfide bond formation occurs for residues facing away from the permeation pathway.

residues has been detailed by Koprowski and Kubalski (2003). Analytical models (Wiggins and Phillips, 2004) describing the contributions of protein-membrane and bilayer deformation to channel gating provide a crucial energetic framework for characterizing these conformational transitions. Together, these studies provide invaluable guidance for the engineering of stable forms of the MscL and MscS open states that will be essential for future progress in the crystallographic analysis of these fundamental mechanosensitive systems.

Acknowledgments

We would like to acknowledge the contributions of Rob Spencer, Geoffrey Chang, Allen Lee, and Meg Barclay in launching the studies described in this chapter, and Yan Poon, Zhenfeng Liu, Chris Gandhi, and Jeff Lai for continuing these efforts. Discussions with Rob Phillips, Eduardo Perozo, Dennis Dougherty, Henry Lester, and Jim Howard are gratefully acknowledged. This work was supported in part by grants from the Howard Hughes Medical Institute and the National Institutes of Health (GM62532) and a postdoctoral fellowship to R.B.B.

References

Akitake, B., Anishkin, A., and Sukharev, S. (2005). The "dashpot" mechanism of stretch-dependent gating in MscS. *J. Gen. Physiol.* **125,** 143–154.

Anishkin, A., and Sukharev, S. (2004). Water dynamics and dewetting transitions in the small mechanosensitive channel MscS. *Biophys. J.* **86,** 2883–2895.

Bass, R. B., and Falke, J. J. (1999). The aspartate receptor cytoplasmic domain: *In situ* chemical analysis of structure, mechanism and dynamics. *Structure* **7,** 829–840.

Bass, R. B., Strop, P., Barclay, M., and Rees, D. C. (2002). The crystal structure of *E. coli* MscS, a voltage-modulated and mechanosensitive channel. *Science* **298,** 1582–1587.

Bass, R. B., Locher, K. P., Borths, E. L., Poon, Y., Strop, P., Lee, A., and Rees, D. C. (2003). The structures of BtuCD and MscS and their implications for transporter and channel function. *FEBS Lett.* **555,** 111–115.

Beckstein, O., and Sansom, M. S. P. (2004). The influence of geometry, surface character, and flexibility on the permeation of ions and water through biological pores. *Phys. Biol.* **1,** 42–52.

Berman, H. M., Westbrook, J., Feng, Z., Gilliland, G., Bhat, T. N., Weissig, H., Shindyalov, I. N., and Bourne, P. E. (2000). The protein data bank. *Nucleic Acids Res.* **28,** 235–242.

Betanzos, M., Chiang, C.-S., Guy, H. R., and Sukharev, S. (2002). A large iris-like expansion of a mechanosensitive channel protein induced by membrane tension. *Nat. Struct. Biol.* **9,** 704–710.

Blount, P., Iscla, I., Li, Y., and Moe, P. C. (2005). The bacterial mechanosensitive channel MscS and its extended family. *In* "Bacterial Ion Channels and their Eukaryotic Homologs" (A. Kubalski and B. Martinac, eds.), pp. 247–258. ASM Press, Washington, DC.

Booth, I. R., and Louis, P. (1999). Managing hypoosmotic stress: Aquaporins and mechanosensitive channels in *Escherichia coli*. *Curr. Opin. Microbiol.* **2,** 166–169.

Booth, I. R., Edwards, M. D., Murray, E., and Miller, S. (2005). The role of bacterial channels in cell physiology. *In* "Bacterial Ion Channels and their Eukaryotic Homologs" (A. Kubalski and B. Martinac, eds.), pp. 291–312. ASM Press, Washington, DC.

Bowie, J. U. (2001). Stabilizing membrane proteins. *Curr. Opin. Struct. Biol.* **11,** 397–402.

Britten, R. J., and McClure, F. T. (1962). The amino acid pool in *Escherichia coli*. *Bacteriol. Rev.* **26,** 292–335.

Butler, S. L., and Falke, J. J. (1996). Effects of protein stabilizing agents on thermal backbone motions: A disulfide trapping study. *Biochemistry* **35,** 10595–10600.

Cantor, R. S. (1999). Lipid composition and the lateral pressure profile in bilayers. *Biophys. J.* **76,** 2625–2639.

Careaga, C. L., and Falke, J. J. (1992). Thermal motions of surface alpha-helices in the D-galactose chemosensory receptor. Detection by disulfide trapping. *J. Mol. Biol.* **226,** 1219–1235.

Chang, G., Spencer, R. H., Lee, A. T., Barclay, M. T., and Rees, D. C. (1998). Structure of the MscL homolog from *Mycobacterium tuberculosis*: A gated mechanosensitive ion channel. *Science* **282,** 2220–2226.

Cruickshank, C. C., Minchin, R. F., LeDain, A. C., and Martinac, B. (1997). Estimation of the pore size of the large-conductance mechanosensitive ion channel of *Escherichia coli*. *Biophys. J.* **73,** 1925–1931.

Deisenhofer, J., Epp, O., Miki, K., Huber, R., and Michel, H. (1985). Structure of the protein subunits in the photosynthetic reaction center of *Rhodopseudomonas viridis* at 3 Å resolution. *Nature* **318,** 618–624.

Denny, M. W. (1993). ''Air and Water: The Biology and Physics of Life's Media.'' Princeton University Press, Princeton, NJ.

Doyle, D. A., Cabral, J. M., Pfuetzner, R. A., Kuo, A., Gulbis, J. M., Cohen, S. L., Chait, B. T., and MacKinnon, R. (1998). The structure of the potassium channel: Molecular basis of K^+ conduction and selectivity. *Science* **280,** 69–77.

Drew, D., Fröderberg, L., Baars, L., and de Gier, J.-W. L. (2003). Assembly and overexpression of membrane proteins in *Escherichia coli*. *Biochim. Biophys. Acta* **1610,** 3–10.

Edmonds, D. T. (2001). ''Electricity and Magnetism in Biological Systems.'' Oxford University Press, Oxford.

Edwards, M. D., Li, Y., Kim, S., Miller, S., Bartlett, W., Black, S., Dennison, S., Iscla, I., Blount, P., Bowie, J. U., and Booth, I. R. (2005). Pivotal role of the glycine-rich TM3 helix in gating the MscS mechanosensitive channel. *Nat. Struct. Mol. Biol.* **12,** 113–119.

Fu, D., Libson, A., Miercke, L. J. W., Weitzman, C., Nollert, P., Krucinski, J., and Stroud, R. M. (2000). Structure of a glycerol-conducting channel and the basis for its selectivity. *Science* **290,** 481–486.

Grisshammer, R., and Tate, C. G. (1995). Overexpression of integral membrane proteins for structural studies. *Q. Rev. Biophys.* **28,** 315–422.

Grisshammer, R., and Tate, C. G. (2003). Preface: Overexpression of integral membrane proteins. *Biochim. Biophys. Acta* **1610,** 1.

Guan, L., Smirnova, I., Verner, G., Nagamori, S., and Kaback, H. R. (2006). Manipulating phospholipids for crystallization of a membrane protein. *Proc. Natl. Acad. Sci. USA* **103,** 1723–1726.

Hamill, O. P., and Martinac, B. (2001). Molecular basis of mechanotransduction in living cells. *Physiol. Rev.* **81,** 685–740.

Hessa, T., White, S. H., and von Heijne, G. (2005). Membrane insertion of a potassium-channel voltage sensor. *Science* **307,** 1427.

Hille, B. (2001). ''Ionic Channels of Excitable Membranes,'' 3rd edn. Sinauer Associates, Sunderland, Massachusetts.

Hutchinson, E. G., and Thornton, J. M. (1996). PROMOTIF—a program to identify and analyze structural motifs in proteins. *Protein Sci.* **5,** 212–220.

Iwata, S. (2003). Crystallization informatics of membrane proteins. *In* ''Methods and Results in Membrane Protein Crystallization'' (S. Iwata, ed.), pp. 281–297. International University Line, La Jolla.

Jiang, Y., Lee, A., Chen, J., Ruta, V., Cadene, M., Chait, B. T., and MacKinnon, R. (2003). X-ray structure of a voltage-dependent K^+ channel. *Nature* **423,** 33–41.

Kantardjieff, K. A., and Rupp, B. (2004). Matthews coefficient probabilities: Improved estimates for unit cell contents of proteins, DNA and protein-nucleic acid complex crystals. *Protein Sci.* **12,** 1865–1871.

Kashino, Y. (2003). Separation methods in the analysis of protein membrane complexes. *J. Chromatogr. B* **797,** 191–216.

Koprowski, P., and Kubalski, A. (2003). C-termini of the *Escherichia coli* mechanosensitive ion channel (MscS) move apart upon the channel opening. *J. Biol. Chem.* **278,** 11237–11245.

Kraulis, P. J. (1991). Molscript—a program to produce both detailed and schematic plots of protein structures. *J. Appl. Crystallogr.* **24,** 946–950.

Kung, C. (2005). A possibly unifying principle for mechanosensation. *Nature* **436,** 647–654.

Kuo, A., Gulbis, J. M., Antcliff, J. F., Rahman, T., Lowe, E. D., Zimmer, J., Cuthbertson, J., Ashcroft, F. M., Ezaki, T., and Doyle, D. A. (2003). Crystal structure of the potassium channel KirBac1. 1 in the closed state. *Science* **300,** 1922–1926.

Lee, S. Y., Lee, A., Chen, J. Y., and MacKinnon, R. (2005). Structure of the KvAP voltage-dependent K^+ channel and its dependence on the lipid membrane. *Proc. Natl. Acad. Sci. USA* **102,** 15441–15446.

Levin, G., and Blount, P. (2004). Cysteine scanning of MscL transmembrane domains reveals residues critical for mechanosensitive channel gating. *Biophys. J.* **86,** 2862–2870.

Levina, N., Tötemeyer, S., Stokes, N. R., Louis, P., Jones, M. A., and Booth, I. A. (1999). Protection of *Escherichia coli* cells against extreme turgor by activation of MscS and MscL mechanosensitive channels: Identification of genes required for MscS activity. *EMBO J.* **18,** 1730–1737.

Long, S. B., Campbell, E. B., and Mackinnon, R. (2005). Crystal structure of a mammalian voltage-dependent Shaker family K^+ channel. *Science* **309,** 897–903.

Martinac, B., Buechner, M., Delcour, A. H., Adler, J., and Kung, C. (1987). Pressure-sensitive ion channel in *Escherichia coli*. *Proc. Natl. Acad. Sci. USA* **84,** 2297–2301.

Matthews, B. W. (1968). Solvent content of protein crystals. *J. Mol. Biol.* **33,** 491–497.

Michel, H. (ed.) (1991). "Crystallization of Membrane Proteins." CRC Press, Boca Raton, FL.

Miyazawa, A., Fujiyoshi, Y., and Unwin, N. (2003). Structure and gating mechanism of the acetylcholine receptor pore. *Nature* **423,** 949–955.

Mura, C., Phillips, M., Kozhukhovsky, A., and Eisenberg, D. (2003). Structure and assembly of an augmented Sm-like archaeal protein 14-mer. *Proc. Natl. Acad. Sci. USA* **100,** 4539–4544.

Murata, K., Mitsuoka, K., Hirai, T., Walz, T., Agre, P., Heymann, J. B., Engel, A., and Fujiyoshi, Y. (2000). Structural determinants of water permeation through aquaporin-1. *Nature* **407,** 599–605.

Murzin, A. G., Lo Conte, L., Ailey, B. G., Brenner, S. E., Hubbard, T. J. P., and Chothia, C. (1995). SCOP: A structural classification of proteins database for the investigation of sequences and structures. *J. Mol. Biol.* **247,** 536–540.

Nelson, P. (2004). "Biological Physics: Energy, Information, Life." W. H. Freeman, New York.

Odahara, T. (2004). Stability and solubiliity of integral membrane proteins from photosynthetic bacteria solubilized in different detergents. *Biochim. Biophys. Acta* **1660,** 80–92.

Pakula, A. A., and Simon, M. I. (1992). Determination of transmembrane protein structure by disulfide crosslinking—the *Escherichia coli* Tar receptor. *Proc. Natl. Acad. Sci. USA* **89,** 4144–4148.

Perozo, E., and Rees, D. C. (2003). Structure and mechanism in prokaryotic mechanosensitive channels. *Curr. Opin. Struct. Biol.* **13,** 432–444.

Perozo, E., Cortes, D. M., Sompornpisut, P., Kloda, A., and Martinac, B. (2002a). Open channel structure of MscL and the gating mechanism of mechanosensitive channels. *Nature* **418,** 942–948.

Perozo, E., Kloda, A., Cortes, D. M., and Martinac, B. (2002b). Physical principles underlying the transduction of bilayer deformation forces during mechanosensitive channel gating. *Nat. Struct. Biol.* **9,** 696–703.

Poolman, B., Blount, P., Folgering, J. H. A., Friesen, R. H. E., Moe, P. C., and van der Heide, T. (2002). How do membrane proteins sense water stress? *Mol. Microbiol.* **44,** 889–902.

Robinson, R. A., and Stokes, R. H. (1959). "Electrolyte Solutions," 2nd edn. Butterworth & Co., London.

Shapovalov, G., and Lester, H. A. (2004). Gating transitions in bacterial ion channels measured at 3 us resolution. *J. Gen. Physiol.* **124,** 151–161.

Shapovalov, G., Bass, R. B., Rees, D. C., and Lester, H. A. (2003). Open-state disulfide crosslinking between *Mycobacterium tuberculosis* mechanosensitive channel subunits. *Biophys. J.* **84,** 2357–2365.

Smart, O. S., Neduvelil, J. G., Wang, X., Wallace, B. A., and Sansom, M. S. (1996). HOLE: A program for the analysis of the pore dimensions of ion channel structural models. *J. Mol. Graph. Model.* **14,** 354–360.

Smart, O. S., Breed, J., Smith, G. R., and Sansom, M. S. P. (1997). A novel method for structure-based prediction of ion channel conductance properties. *Biophys. J.* **72,** 1109–1126.

Spencer, R. H., and Rees, D. C. (2002). The α-helix and the organization and gating of channels. *Annu. Rev. Biophys. Biomol. Struct.* **31,** 207–233.

Spencer, R. H., Chang, G., Bass, R. B., and Rees, D. C. (2003). Crystallization and structure determination of MscL, A gated prokaryotic mechanosensitive channel. *In* "Methods and Results in Membrane Protein Crystallization" (S. Iwata, ed.), pp. 241–251. International University Line, La Jolla.

Stokes, N. R., Murray, H. D., Subramaniam, C., Gourse, R. L., Louis, P., Bartlett, W., Miller, S., and Booth, I. R. (2003). A role for mechanosensitive channels in survival of stationary phase: Regulation of channel expression by RpoS. *Proc. Natl. Acad. Sci. USA* **100,** 15959–15964.

Stowell, M. H. B., and Rees, D. C. (1995). Structure and stability of membrane proteins. *Adv. Protein Chem.* **46,** 279–311.

Strop, P., Bass, R. B., and Rees, D. C. (2003). Prokaryotic mechanosensitive channels. *Adv. Protein Chem.* **63,** 177–209.

Sukharev, S. (2002). Purification of the small mechanosensitive channel of *E. coli* (MscS): The subunit structure, conduction and gating characteristics in liposomes. *Biophys. J.* **83,** 290–298.

Sukharev, S., and Corey, D. P. (2004). Mechanosensitive channels: Multiplicity of families and gating paradigms. *Sci. STKE* DOI:10. 1126/stke. 2332004eg7.

Sukharev, S., Betanzos, M., Chiang, C.-S., and Guy, H. R. (2001a). The gating mechanism of the large mechanosensitive channel MscL. *Nature* **409,** 720–724.

Sukharev, S., Durell, S. R., and Guy, H. R. (2001b). Structural models of the MscL gating mechanism. *Biophys. J.* **81,** 917–936.

Sukharev, S., Anishkin, A., Chiang, C.-S., Betanzos, M., and Guy, H. R. (2005). MscL, a bacterial mechanosensitive channel. *In* "Bacterial Ion Channels and their Eukaryotic Homologs" (A. Kubalski and B. Martinac, eds.), pp. 259–290. ASM Press, Washington, DC.

Sukharev, S. I., Blount, P., Martinac, B., Blattner, F. R., and Kung, C. (1994). A large-conductance mechanosensitive channel in *E. coli* encoded by *mscl* alone. *Nature* **368,** 265–268.

Sukharev, S. I., Blount, P., Martinac, B., and Kung, C. (1997). Mechanosensitive channels of *Escherichia coli*: The MscL gene, protein, and activities. *Annu. Rev. Physiol.* **59,** 633–657.

Sukharev, S. I., Sigurdson, W. J., Kung, C., and Sachs, F. (1999). Energetic and spatial parameters for gating of the bacterial large conductance mechanosensitive channel, MscL. *J. Gen. Physiol.* **113,** 525–539.

Terpe, K. (2003). Overview of tag protein fusions: From molecular and biochemical fundamentals to commerical systems. *Appl. Microbiol. Biotechnol.* **60,** 523–533.

Weiss, T. F. (1996). "Cellular Biophysics, Vol. I: Transport." MIT Press, Cambridge, MA.

White, S. H. (2004). The progress of membrane protein structure determination. *Protein Sci.* **13,** 1948–1949.

Wiggins, P., and Phillips, R. (2004). Analytic models for mechanotransduction: Gating a mechanosensitive channel. *Proc. Natl. Acad. Sci. USA* **101,** 4071–4076.

Wu, J. H., and Kaback, H. R. (1996). A general method for determining helix packing in membrane proteins *in situ*: Helices I and II are close to helix VII in the lactose permease of *Escherichia coli*. *Proc. Natl. Acad. Sci. USA* **93,** 14498–14502.

Zeidel, M. L., Ambudkar, S. V., Smith, B. L., and Agre, P. (1992). Reconstitution of functional water channels in liposomes containing purified red cell CHIP28 protein. *Biochemistry* **31,** 7436–7440.

Zhang, H., Kurisu, G., Smith, J. L., and Cramer, W. A. (2003). A defined protein-detergent-lipid complex for crystallization of integral membrane proteins: The cytochrome b_6f complex of oxygenic photosynthesis. *Proc. Natl. Acad. Sci. USA* **100,** 5160–5163.

Zhou, Y., Morais-Cabral, J. H., Kaufman, A., and MacKinnon, R. (2001). Chemistry of ion coordination and hydration revealed by a K^+ channel-Fab complex at 2.0 Å resolution. *Nature* **414,** 43–48.